# Compliant Realignment of Binding Sites in Muscle: Transient Behavior and Mechanical Tuning

Thomas L. Daniel,* Alan C. Trimble,* and P. Bryant Chase#

*Department of Zoology, University of Washington, Seattle, Washington 98195-1800, and #Departments of Radiology and Physiology and Biophysics, University of Washington, Seattle, Washington 98195-7115 USA

ABSTRACT The presence of compliance in the lattice of filaments in muscle raises a number of concerns about how one accounts for force generation in the context of the cross-bridge cycle—binding site motions and coupling between cross-bridges confound more traditional analyses. To explore these issues, we developed a spatially explicit, mechano-chemical model of skeletal muscle contraction. With a simple three-state model of the cross-bridge cycle, we used a Monte Carlo simulation to compute the instantaneous balance of forces throughout the filament lattice, accounting for both thin and thick filament distortions in response to cross-bridge forces. This approach is compared to more traditional mass action kinetic models (in the form of coupled partial differential equations) that assume filament inextensibility. We also monitored instantaneous force generation, ATP utilization, and the dynamics of the cross-bridge cycle in simulations of step changes in length and variations in shortening velocity. Three critical results emerge from our analyses: 1) there is a significant realignment of actin-binding sites in response to cross-bridge forces, 2) this realignment recruits additional cross-bridge binding, and 3) we predict mechanical behaviors that are consistent with experimental results for velocity and length transients. Binding site realignment depends on the relative compliance of the filament lattice and cross-bridges, and within the measured range of these parameters, gives rise to a sharply tuned peak for force generation. Such mechanical tuning at the molecular level is the result of mechanical coupling between individual cross-bridges, mediated by thick filament deformations, and the resultant realignment of binding sites on the thin filament.

## INTRODUCTION

Until quite recently, experimental and theoretical analyses of muscle contraction have assumed that both thick and thin filaments are inextensible (e.g. Ford et al., 1981; Bagni et al., 1990). Thus, even though tens to hundreds of motor molecules (myosin) produce forces on each thin filament, an assumption of filament inextensibility suggests that mass action kinetics could form a reasonable model of the cross-bridge cycle. Such approaches are appropriate as long as each cross-bridge behaves independently. By this scheme, therefore, force generation can be calculated by summing the average state (e.g., bound versus unbound) of independently acting cross-bridges. However, as has recently been shown (Huxley et al., 1994; Wakabayashi et al., 1994; Goldman and Huxley, 1994), both thick and thin filaments are indeed compliant, with as much as 70% of the total compliance of the sarcomere residing in the filaments per se rather than in the cross-bridges. Accordingly, current interpretations of the cross-bridge cycle, as well as possible mechanical coupling between cross-bridges, needs reexamination, because cross-bridge distortions, binding site availability to cross-bridges, and the kinetics of force generation are all likely tied to the presence of compliance within filament lattice.

Recent experimental approaches aimed at unraveling the role of compliance in the dynamics of force generation have emphasized the relationship between muscle fiber stiffness and cross-bridge attachment (Higuchi et al., 1995). These experiments, combined with both direct and indirect measures of filament compliance and distortions in muscle fibers (Huxley et al., 1994; Wakabayashi et al., 1994; Kojima et al., 1994), all point to an important role for filament compliance in modulating cross-bridge dynamics. Indeed, the strongly nonlinear relationship between muscle fiber stiffness and sarcomere length (Higuchi et al., 1995) provides a compelling case for a need to probe more deeply into the mechanics of force generation in a compliant lattice of filaments and to reexamine the theoretical approaches that have formed the underpinnings of our analyses of the cross-bridge cycle.

The more traditional theoretical analyses that have used mass action kinetics are hampered by several limitations that arise in the presence of filament compliance. First, cross-bridge state transitions are no longer independent of cross-bridge force generation and history of cross-bridge attachment and detachment. The notion that cross-bridges are independent actuators, therefore, may be violated. For example, even in isometric conditions, binding sites on compliant thin filaments could move in response to cross-bridge forces. Such cross-bridge-induced motions can, in

*Received for publication 18 October 1996 and in final form 8 January 1998.*

Address reprint requests to Dr. T. L. Daniel, Department of Zoology, Box 351800, University of Washington, Seattle, WA 98195-1800. Tel.: 206-543-1659; Fax: 206-543-3041: E-mail: danielt@zoology.washington.edu.



0006-3495/98/04/1611/11 $2.00

turn, change the likelihood of cross-bridge attachment and detachment. Accordingly, any theoretical analysis must account for both temporal (kinetic) and spatial (motion) dynamics of the cross-bridge cycle.

Several of these issues have recently been examined with a partial differential equation analysis of a two-state model by Mijailovich et al. (1996). Their analysis shows that local deformations of thin filaments (and their binding sites) as well as mechanical coupling between cross-bridges can, indeed, play crucial roles in the dynamics of force generation and the determinants of fiber stiffness. Here we develop a parallel theoretical framework that accounts for compliance in the context of the mechanical coupling between cross-bridges. Our approach differs, however, from that of Mijailovich et al. (1996) in several regards. Here we are interested in probing how compliance affects the time history of force generation in response to a variety of transient conditions, including length transients. We are also interested in understanding how the geometry of the filament lattice determines force generation in the context of filament compliance. As such, we also develop a spatially explicit model that accounts for the locations of all binding sites and cross-bridges in a two-filament (one thick and one thin) system. It is important to note that although a two-filament model does not represent the complete three-dimensional structure of thin and thick filaments in a muscle, it provides a simple system for asking whether compliance plays any role in the dynamics of force generation, as well as a method by which we can directly compare a spatially explicit model with previous mass action models that investigate two-filament interactions.

Our analyses, therefore, are divided into two portions: 1) a system of partial differential equations that describes cross-bridge interactions with rigid filaments and forms a reference behavior, against which we compare 2) predictions of a spatially explicit model in which the filament compliance is not zero and can be varied. The spatially explicit model is developed as a Monte Carlo process. By this scheme, we examine stochastic (thermally driven) fluctuations of every cross-bridge to compute state transitions. Although computationally time consuming, this approach lends itself to a simple mathematical framework that is easily adapted to a variety of scenarios, including arbitrary motions, temporal transients, and geometric (sarcomere length) variations. Indeed, Monte Carlo methods have proved quite useful in modeling a variety of molecular events (Fichthorn and Weinber, 1991), including those associated with motor molecules (Cordova et al., 1992). Here we use both the partial differential and Monte Carlo type models to examine the dynamics of force generation for a three-state cross-bridge cycle to ask: 1) How does filament compliance alter our interpretation of cross-bridge attachment and detachment, and 2) How does the total force generated by muscle depend upon the mechanical properties of both the filaments and motor proteins?

## MODEL DEVELOPMENT

We develop here two models based on a three-state cross-bridge cycle. The first and central model is a spatially explicit system of equations that accounts for filament compliance and mechanical coupling between cross-bridges. It includes both temporal and spatial transients that can be imposed on muscle fibers. The second model is a modest revision of current mass action kinetic models that accounts for simultaneous temporal and mechanical transients in the form of a system of partial differential equations. This model not only serves as a comparison for the spatially explicit mode; it also sheds light on how compliance may alter the dynamics of cross-bridge cycling.

### A spatially explicit model

Our analysis is based on a model of a half-sarcomere (Fig. 1) composed of just two filaments with a geometry that is consistent with the average spacings measured in vertebrate striated muscle (Higuchi et al., 1995). Thus, for a half-sarcomere, we construct a thick filament with 20 myosin heads (42.9 nm apart under zero load) that face a single thin filament. The thick filament has an undecorated zone of 80 nm (half the M-line), giving a total rest length of 1.79 $\mu$m

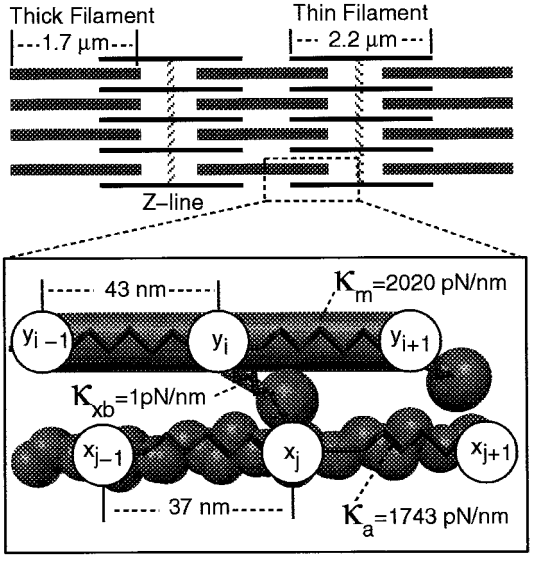


FIGURE 1 A schematic diagram of the geometric and mechanical arrangement of interacting cross-bridges. Dimensions of thin and thick filaments for vertebrate striated muscle (Higuchi et al., 1995) were used in the computations, along with estimates of the spacing of cross-bridges and binding sites that are colinear (those cross-bridges and binding sites that face two adjacent filaments). Therefore, the node locations ($y_i$ and $x_j$) are, respectively, 43 and 37 nm apart when no forces act on either filament. The spring constants for the thick filament ($\kappa_m$), thin filament ($\kappa_a$), and cross-bridges ($\kappa_{xb}$) were derived from recent experimental observations (see text). The stiffness of the undecorated zone of the thick filament is assumed to be the same as that with cross-bridges extending. The *z*-disk compliance is treated as one additional thin-filament spring in series with those between binding sites. In the model, the entire thick filament consists of 20 such units, whereas the thin filament consists of 30 repeated units.

for the full thick filament. The thin filament has a length of 1.1 $\mu$m, with 30 colinear binding sites, with a separation of 37.3 nm between sites, forming a set of binding locations that face a single thick filament. This measure of binding site spacing is also consistent with experimental values observed by Molloy et al. (1995b). Thin filaments, thick filaments, and cross-bridges are all represented as linear springs. Because inertia and viscosity are presumed negligible, this simple arrangement of linear springs is amenable to a force balance in the form of a linear system of simultaneous equations. Thus an instantaneous force balance for $N$ cross-bridges and $M$ actin-binding sites can be formed for every binding site and every cross-bridge. For example, with the $i$th bound cross-bridge and the $j$th binding site (see Fig. 1), we set the sum of forces (each force is the product of the spring constant and the local distortion) to be zero about any point:

$$\kappa_m(y_{i+1} - y_i - m_s) + \kappa_{xb,i}(x_j - y_i) - \kappa_m(y_i - y_{i-1} - m_s) = 0$$

$$\kappa_a(x_{j+1} - x_j - a_s) - \kappa_{xb,i}(x_j - y_i) - \kappa_a(x_j - x_{j-1} - a_s) = 0. \quad (1)$$

where $\kappa_m$, $\kappa_a$, and $\kappa_{xb}$ are, respectively, the spring constants for thick filaments, thin filaments, and cross-bridges; $x_j$ is the location of the $j$th binding site on thin filaments; $y_i$ is the location of the $i$th cross-bridge point of attachment to the thick filament ($i = 1 \ldots N$; $j = 1 \ldots M$); and $m_s$ and $a_s$ are, respectively, the spacings between adjacent myosin heads and actin binding sites for an unloaded filament. This force balance leads to a system of $N + M$ linear equations with $N + M$ unknowns (the locations of all nodes $x_j$ and $y_i$). Solving such a system requires that we formulate and solve the matrix equation

$$\underline{\mathbf{K}} \cdot \mathbf{Z} = \mathbf{A} \quad (2)$$

where $\underline{\mathbf{K}}$ is a matrix of spring constants, $\mathbf{Z}$ is the vector of locations $\{x_1, x_2, \ldots x_M, y_1, y_2 \ldots y_N\}$, and $\mathbf{A}$ is a vector that contains rest lengths and directions for end motions of the system.

Values for the above spring constants are derived from several recent studies. We use the estimate of 65 pN/nm for a 1-$\mu$m-long thin filament (Kojima et al., 1994). With 37.3 nm between thin filament binding sites, therefore, we scale this to a local spring constant ($\kappa_a$) of 1743 pN/nm. Similarly, because Wakabayashi et al. (1994) suggest that the stiffness of thick filaments is ~150% that of thin filaments, we scaled the thick filament stiffness accordingly to yield a value of 2020 pN/nm for the spring constant of the thick filament ($\kappa_m$). Whereas estimates of cross-bridge stiffness vary in the range of 0.1 to ~10 pN/nm, we chose a conservative estimate of 1 pN/nm (Finer et al., 1994; Molloy et al., 1995a). For unbound cross-bridges, the spring constant $\kappa_{xb}$ is set to 0.

In addition to estimates of the spring constants, Eq. 1 also requires kinetic rules for cross-bridge binding to determine force generation. We are concerned here with how compliance affects the dynamics of force generation and thus choose to focus on a model with only three states (Fig. 2). More complex models are certainly available (e.g., Piazzesi and Lombardi, 1995), but for understanding the consequences of variation in filament compliance, we seek to use the fewest number of states for mechanical calculations. Although two-state models are more attractive mathematically, many recent studies (Dantzig et al., 1992; Homsher and Lacktis, 1988; as well as the discussion in Huxley and Simmons, 1971) point to strong evidence for including a minimum of three states in the cross-bridge cycle. As such, rather than posing a large number of states to recover rich dynamics, we ask whether a few coupled states can achieve the same goal.

Following previous analyses (Pate and Cooke, 1989), we established functions for the free energy of each of the three states. Using a reference energy of 0 for the unbound state, the remaining two states have energy functions (in $RT$s) that are parabolic with cross-bridge distortion:

$$G_1 = 0; \quad (3a)$$

$$G_2 = -4.3 - \kappa'_{xb}(x - x_o)^2; \quad (3b)$$

$$G_3 = -4.3 - \kappa'_{xb}(x)^2 + \log(1.89\ 10^{-4}[P_i]) \quad (3c)$$

where $G$ is the energy level of each state, $\kappa'_{xb}$ is the cross-bridge spring constant (in $RT$/nm$^2$), $x$ is the distance to a binding site, $x_o$ is the distortion of a cross-bridge induced by ATP hydrolysis, and $[P_i]$ is the intracellular free phosphate concentration (2 mM; Kushmerick et al., 1992; Dantzig et al., 1992; Pate and Cooke, 1989). The strain energy of the cross-bridge with a 7-nm extension corresponds to ~50% of the free energy of ATP hydrolysis. The 7-nm offset in rest length is removed upon $P_i$ release in the transition from state

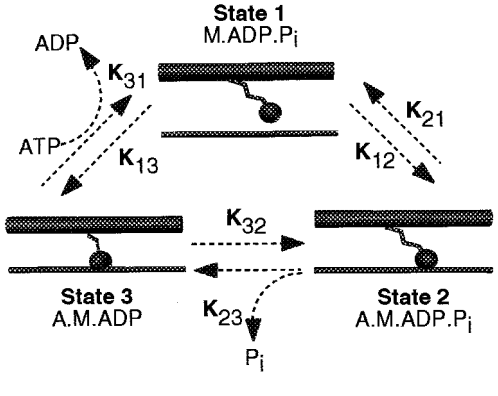


FIGURE 2 The three-state model for the cross-bridge cycle is shown diagrammatically. State 1: Detached myosin (M) cross-bridge with ADP + $P_i$, with the hydrolysis of the phosphate leading to a positive (*to the right in this figure*) strain in the cross-bridge of 7 nm. State 2: Myosin weakly bound to an actin-binding site. State 3: The phosphate is released from the cross-bridge to create a strongly bound state with the 7-nm offset removed. The set of biochemical states leading to the substitution of ATP with ADP and its subsequent hydrolysis are lumped into the transition from state 3 to state 1.

2 to state 3, favoring force generation in the forward reaction (Fig. 2).

With the above estimates of the total free energy, we calculate the forward rate functions to complete the analysis, with reverse rates calculated from equilibrium thermodynamics: $r_{ij}/r_{ji} = \exp[(G_i - G_j)/RT]$. Each rate calculation is described below, with the notion that state 2 corresponds to a weakly bound state and state 3 is strongly bound.

The rate function associated with attachment of cross-bridges to actin ($r_{12}$) is derived from a thermal forcing calculation (Kramers, 1940; Papoulis, 1991; Hunt et al., 1994). By this scheme, an instantaneous force balance for a myosin head subject to thermal fluctuations provides the basis for the analysis. At any instant in time, the myosin head is subject to thermal forcing. This force is balanced, instantaneously, by a restoring spring force ($\kappa_{xb}[z - z_o]$), a viscous force retarding the motion of the myosin head ($f\ dz/dt$), and an inertial force ($m\ d^2z/dt^2$):

$$m\ d^2z/dt^2 + f\ dz/dt + \kappa_{xb}(z - z_o) = F(t) \qquad (4)$$

where $m$ is the mass of the sphere, $z$ is the location of the sphere ($z_o$ is its rest location), $f$ is the viscous drag ($f = 6\pi r\mu$; $r$ is the radius of a cross-bridge (= 5 nm); $\mu$ is the viscosity of water), and $F(t)$ is the thermal forcing function, whose power spectrum is $2RTf$. From the power spectra of each side of Eq. 4, the probability density function for a myosin head being in any distortion ($z$) is computed as a function of the spring constant ($\kappa_{xb}$) for the tether (after analyses by Kramers, 1940; Papoulis, 1991; Hunt et al., 1994):

$$P(x) = [\kappa'_{xb}/2\pi RT]^{1/2}\exp[-\kappa'_{xb}(z - z_o)^2/(2RT)] \qquad (5)$$

This probability density function is multiplied by 1000 nm $s^{-1}$ to obtain attachment rates that yield physiological force-velocity behavior and net ATP hydrolysis rate (~1 ATP/cross-bridge/s; Glynn and Sleep, 1985; Chase and Kushmerick, 1995). This formulation of attachment provides a direct connection between the cross-bridge spring constant, force generation, and the likelihood for attachment. The remaining two transition rates ($r_{23}$ and $r_{31}$) followed from earlier analyses (Pate and Cooke, 1989) and depend on cross-bridge distortion:

$$r_{12} = 1000[\kappa'_{xb}/2\pi RT]^{1/2}\exp[-\kappa'_{xb}(x - x_o)^2/(2RT)] \qquad (6a)$$

$$r_{23} = 1000 + 5000/\exp(x) \qquad (6b)$$

$$r_{31} = x > 0\text{: } 2x; \qquad x \le 0\text{: } -100x \qquad (6c)$$

The numerical constants in the above equations are set to have units that give appropriate dimensions in the rate functions. Thus, in Eq. 6b, distortion is normalized to 1 nm, and the two numerical constants have units of $s^{-1}$. In Eq. 6c, the numerical constants have units of nm/s.

Although myriad strain dependencies can be posed, this particular set gives reasonable force-velocity behaviors (see Simulation Results). We follow Pate and Cooke's (1989) assumption that in the unbound state, the cross-bridge binds favorably in a forward position (~7 nm), and after the release of $P_i$, that 7-nm offset is removed, and $x_o = 0$ corresponds to the strain-free position of the cross-bridge. Such a 7-nm offset corresponds to approximately a 50% efficiency in the conversion of ATP energy (one hydrolysis of phosphate) to mechanical energy. Moreover, the change in rest length drives the free energy changes in a direction that favors force generation through the cross-bridge cycle.

We use a Monte Carlo simulation to compute instantaneous force development and ATPase rates. At each time step of duration $\delta t$, the state of each cross-bridge is examined, and the probability of a transition is computed from the distortion of the cross-bridge if bound (states 2 and 3), or from the distance to a binding site if unbound (state 1). For an unbound cross-bridge, the search algorithm seeks the two nearest available binding sites. For these binding sites, the probability of binding is computed from the rate constants ($p_{12} = \delta t r_{12}$). Thus the probability of binding to either of these sites is calculated, and the larger of these probabilities is used in computing the likelihood of attachment (using $\kappa_{xb}$ = 1 pN/nm in Eq. 6a, a myosin head effectively needs to be within 2 nm of a possible binding site to have any appreciable probability of attachment—those myosin heads residing in the intervening space (>2 nm) have such low binding likelihoods as not to affect any computational results). If that probability exceeds a random number generated at that time step, binding occurs.

For a bound cross-bridge there are three possible situations: 1) it may undergo a forward transition with probability $r_{ij}\delta t$; 2) it may undergo a reverse transition with probability $r_{ji}\delta t$; or 3) it may remain in its current state with probability $1 - \delta t(r_{ij} + r_{ji})$. To simulate this set of situations we use a two-tailed probability function to determine the likelihood of either forward or reverse transitions giving rise to three intervals:

reverse transition: $[0 \ldots P_{ji}]$
no change: $[P_{ji} \ldots (1 - P_{ij})]$
forward transition: $[(1 - P_{ij}) \ldots 1]$

Thus the right tail of the distribution corresponds to a forward transition, the left tail corresponds to a reverse transition, and the central lobe of the distribution corresponds to no change of state. At each time step we compute $P_{ji}$ and $1 - P_{ij}$ and compare these values to a random number (between 0 and 1). The state transition is determined by where, in the above three intervals, the random number falls.

Once the new state and distortion of each cross-bridge are calculated from the above algorithm, we then solve at that time step the instantaneous force balance (Eq. 2) to compute a new distribution of myosin heads and binding sites. Our set of 20 cross-bridges and 30 thin filament binding sites gives rise to a 20 × 30 matrix for which we use L-U decomposition and back-substitution algorithms in the matrix solution. The distance to a binding site is computed for each cross-bridge at each time step before solving the matrix for the relative locations of binding sites ($x_j$) and cross-bridges ($y_i$).

The step size in the algorithm is selected to give a dwell time in any state for any cross-bridge of ~10 time steps. As such, our typical simulation step size was set at 10 $\mu$s for a total simulation duration of 0.5 s. The simulations were launched from an initial condition in which all cross-bridges were unbound and all binding sites were available (fully activated thin filament). Because of the stochastic nature of this model, we ran 50 independent trials and averaged the predicted instantaneous force and total ATP utilization. Unlike traditional mass action models, which compute the force by summing the contribution of all bound cross-bridges, we computed the force on the first series spring in the thick filament (see Fig. 1).

### The mass-action model

Under an assumption of inextensibility in the filaments, we can use the above three-state model and its state transitions to derive an equivalent mass action model. We include this to provide a direct comparison between our spatially explicit model and mass action approaches that have commonly been used (e.g., Pate and Cooke, 1989; Mijailovich et al. 1996). We thus formulate continuous equations that are integrated over the domain of one binding site repeat to account for the Vernier effect of misregistration in investigating the limiting behavior of rigid filament systems. Below we account for both spatial and temporal transients with a coupled system of partial differential equations. With three states for the cross-bridge cycle, our analysis is an expanded version of the recent two-state model of Mijailovich et al. (1996) and is consistent with the cycle formulation we have used above.

In deriving the equations, we must account for two mechanisms by which a set of cross-bridges in a particular state and location enters or leaves that set; one is driven by state transitions, and the other by motion (convection). In a standard formulation (Bird et al., 1960) these fluxes of cross-bridges may be combined to describe both the spatial and temporal dynamics of the fraction bound in each state as a hyperbolic, flux conservative equation:

$$\partial \mathbf{n}/\partial t = \mathbf{K} \cdot \mathbf{n} - \partial(V(t)\mathbf{n})/\partial x \tag{7}$$

where $\mathbf{n}$ is a vector representing the fraction of cross-bridges in each state ($= \{n_1, n_2, n_3\}$), $\mathbf{K}$ is the matrix of transition rates, and $V(t)$ is the instantaneous shortening velocity. With the condition that $\Sigma n_i = 1$, the system of three simultaneous equations for the three states reduces to two with an offset vector ($\mathbf{u}$):

$$\partial \mathbf{n}/\partial t = \mathbf{K} \cdot \mathbf{n} + u - \partial(V(t)\mathbf{n})/\partial x$$

$$\mathbf{n} = \{n_2, n_3\}$$

$$\mathbf{u} = \{r_{12}, r_{13}\}$$

$$\mathbf{K} = \begin{matrix} -(r_{12} + r_{21} + r_{23}), & (r_{32} - r_{12}) \\ (r_{23} - r_{13}), & -(r_{31} + r_{32} + r_{13}) \end{matrix} \tag{8}$$

Equation 7 has two limiting behaviors: 1) for isometric conditions ($V(t) = 0$), the rightmost term vanishes and we recover the familiar system of ordinary differential equations for a cross-bridge cycle; 2) for constant shortening velocity, the rate of change of cross-bridges occupying any one state with any one average distortion is zero ($\partial n/\partial t = 0$). In this latter case, the resultant ordinary differential equations are identical to those used by Pate and Cooke (1989) for computing force-velocity relationships. In its full form, Eq. 7 permits simulation of both temporal and motion (spatial) transients.

Importantly, Eq. 8 also gives some insight into the possible contributions of filament compliance to the dynamics of the cross-bridge cycle. Expansion of the rightmost term gives rise to the following:

$$\partial \mathbf{n}/\partial t = \mathbf{K} \cdot \mathbf{n} - V(x, t)\partial \mathbf{n}/\partial x - \mathbf{n}\partial V(x, t)/\partial x \tag{9}$$

The first right-hand term in Eq. 9 contains the traditional flux balance due to state transitions, and the second term contains the spatial flux due to motion. The third term, however, contains the contribution of filament distortion (dilation or compression of binding sites) to the total balance of fluxes. This is because it measures the spatial gradient in the motion of binding sites ($\partial V(x, t)/\partial x$). If, as shown above, there is no dilation, the spatial gradient of the motion is identically zero. However, in the presence of nonzero compliance, such a spatial gradient can exist. For example, a strain rate gradient of only 100 $s^{-1}$ could have profound consequences for our accounting of filament compliance, essentially introducing another "state" into the problem. This result highlights the potential importance of compliance in either mass action or spatially explicit models.

It is critical to note, however, that the strain rate gradient ($\partial V(x, t)/\partial x$) in Eq. 9 depends upon how many cross-bridges are bound to the thin filament and their specific location. Furthermore, because the geometry of binding sites and cross-bridges is unspecified in such models, in the presence of compliance, solutions to Eq. 9 are not possible, even with numerical schemes. However, with zero compliance (rigid filaments) the gradient term is zero and the equations, although nonlinear, can be solved numerically. Here we use this zero compliance condition to compare mass-action (rigid filament) models against our spatially explicit model with compliance.

We developed a numerical method to solve Eq. 9 (with zero compliance) based on implicit time differencing and an upwind spatial differencing scheme (Press et al., 1992). We computed, therefore, the fraction of cross-bridges bound in each state. In turn, we use these fractions, along with the spring constant of the cross-bridge, to compute the total force by integration over all possible binding sites, accounting for the Vernier effect of binding site distribution:

$$F(t) = 1/a_s \int_{-a_s/2}^{+a_s/2} \kappa_{xb}(n_2(x - x_o) + n_3(x))\mathrm{d}x \tag{10}$$

## SIMULATION RESULTS: MODEL TESTING

Here we compare our spatially explicit, compliant model and our mass action model (with zero compliance) to examine the consequences of filament compliance for dynamics of force generation. We use several tests, drawing heavily on published experimental observations of the mechanical behavior of active muscle.

### Peak deformations within the lattice and periodicity changes

Two recent x-ray diffraction studies of striated muscle (Huxley et al., 1994; Wakabayashi et al., 1994) showed significant periodicity changes in thin filament structure during maximum tension generation. In particular, the actin monomer spacing increased by ~0.2–0.3% from an initial value of ~2.7 nm. For a thin filament 1 $\mu$m long, maximum activation would lead, therefore, to a length change of ~2 nm in all. Our simulation, using separate data for thin filament compliance (65 pN/nm for a 1-$\mu$m thin filament; Kojima et al., 1994), shows a much more conservative value for thin filament deformation (0.2 nm, Fig. 3), whereas a 10-fold increase in filament compliance more closely matches the 2-nm measurement. Several factors, however, are critical in understanding this difference. First, our model examines only the interaction of one thin filament with one thick filament. In reality, however, each thin filament interacts with cross-bridges from three thick filaments, giving rise to three times the total force. Furthermore, Isambert et al. (1995) indicate that the compliance of the thin filament may strongly depend upon its level of activation. For a regulated thin filament (with tropomyosin and troponin), the stiffness can fall by a factor of ~3 when calcium is present. This additional decrement in the stiffness, combined with the threefold amplification of force due to the actin-myosin ratio, leads to a total distortion of 1.8 nm, far more consistent with the measured value of ~2 nm.

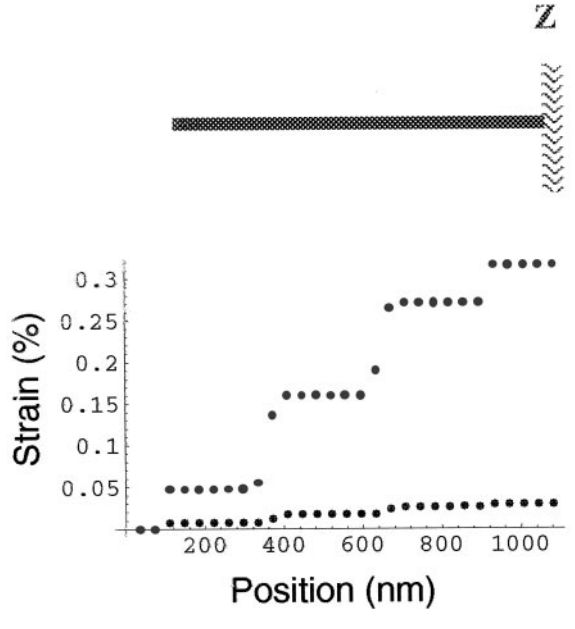


FIGURE 3 Calculated strain (% local distortion) along the thin filament for a thin filament spring constant of 1743 pN/nm (*black dots*; Kojima et al., 1994) and for a spring constant of 174.3 pN/nm (*gray dots, bottom*). The more compliant value (lower spring constant) gives an average strain that is consistent with the x-ray data from Huxley et al. (1994) and Wakabayashi et al. (1994). In both cases, the strain is highly nonuniform, with discontinuities corresponding to binding locations of cross-bridges. Because of the stochastic nature of our simulations (and that of thermal force cross-bridges), the strain inhomogeneities are not pure step functions.

For any nonzero level of compliance in the filament lattice, our results show an important inhomogeneity in thin filament strain (Fig. 3). At the left (free) end of the thin filament (see Fig. 1), where no cross-bridges bind, there is logically no strain (also with zero compliance, there is, of course, no strain anywhere in the thin filament: the *abscissa* in Fig. 3). As cross-bridge forces accumulate along the thin filament toward the *z* disk, strain rises nonuniformly. Each increase is associated with the accumulation of force from one additional cross-bridge. Note that the strain jump associated with the binding of each additional cross-bridge varies along the thin filament, with larger values occurring on the interior of the thin filament. Because the force borne by each cross-bridge is directly proportional to that strain difference, our results also show a spatial inhomogeneity in cross-bridge forces. Such inhomogeneities in cross-bridge forces are problematical for mass action models that assume no dependence on location along a thin filament.

A key issue here is that compliance introduces a realignment of binding sites in response to cross-bridge forces, as seen with the strain distribution in the thin filament (Fig. 3). Thus local binding site motion could be crucial for understanding the dynamics and mechanics of the cross-bridge cycle, a result consistent with that of Mijailovich et al. (1996).

### Energetics, isometric tension, and fractional binding

The filament distortions resulting from cross-bridge forces noted above have two important consequences. First, greater compliance generally leads to greater isometric force generation (Table 1). This result follows from a greater probability of attachment with increased compliance. Moreover, we predict a rather conservative range of attachment probabilities (~0.2–0.3) with rather significant changes in isometric force. A second result is that, over a rather broad range of filament compliance values, we predict a conservative range of ATPase rates (between one and three ATP/cross-bridge/s) that agrees nicely with experimentally observed values (Chase and Kushmerick, 1995; Crow and Kushmerick, 1982).

Intriguingly, although greater compliance is generally manifested as greater tension and higher binding probability, that increased tension occurs with a disproportionately higher ATP utilization rate. Thus compliance not only af-

**TABLE 1 Predictions from the Monte Carlo simulations for isometric force generation**

| SL | Thin compliance | Thin stiff | ATPase | To | To/ATP | $P_{binding}$ | $x_b$ dist. |
|---|---|---|---|---|---|---|---|
| 2.5 | 0.1 | 10.0 | 1.26 | 12.87 | 10.23 | 0.19 | 1.36 |
| 2.5 | 1.0 | 1.0 | 1.09 | 12.68 | 11.63 | 0.19 | 1.40 |
| 2.5 | 10.0 | 0.1 | 1.58 | 16.18 | 10.22 | 0.22 | 1.47 |
| 2.5 | 100.0 | 0.01 | 3.63 | 20.24 | 5.57 | 0.31 | 1.61 |
| 2.2 | 0.01 | 100.0 | 1.85 | 17.08 | 9.23 | 0.26 | 1.82 |
| 2.2 | 0.1 | 10.0 | 1.89 | 19.45 | 10.28 | 0.27 | 1.82 |
| 2.2 | 1.0 | 1.0 | 2.01 | 19.80 | 9.83 | 0.27 | 1.82 |
| 2.2 | 10.0 | 0.1 | 2.08 | 20.20 | 9.73 | 0.27 | 1.71 |
| 2.2 | 100.0 | 0.01 | 4.02 | 21.66 | 5.39 | 0.31 | 1.69 |

We varied sarcomere length (SL in $\mu$m; 2.2 and 2.5) and the stiffness of the thin filament (Thin stiff: varied from 10, 1, 0.1 and 0.01 times the value reported by Kojima et al. (1994)). We monitored the ATPase rate (ATP/cross-bridge/s), the total tension (To in pN), the efficiency of contraction (To/ATP/cross-bridge/s), the mean binding probability ($P_{binding}$ = fraction bound), and the mean distortion of bound cross-bridges ($x_b$ dist in nm). We note increased tension with increased compliance (lower stiffness), but only at the expense of increased ATP utilization. The variances in the mean tension data are all ~0.8 pN.

fects the tension developed, but also the "efficiency" of contraction (tension/ATP/cross-bridge/s; see Crow and Kushmerick, 1982). Because our model deals explicitly with the filament geometry, we can probe this interaction of sarcomere length and compliance in a way that is not easily done with a mass action modeling approach. Indeed, for a sarcomere length of 2.5 $\mu$m, there is a local maximum for the efficiency of contraction that corresponds to the stiffness estimates from Kojima et al. (1994); for a 2.2-$\mu$m sarcomere length, this maximum occurs with stiffer thin filaments.

The above results show a clear dependence of isometric tension on sarcomere length. This dependence is further illustrated by a simulation of isometric tension for a wide range of sarcomere lengths showing results similar to those reported by Gordon et al. (1966) (Fig. 4). In our results, there is a plateau region between 2.0-$\mu$m and 2.3-$\mu$m sarcomere length. The tension declines to zero at a sarcomere length of 3.7 $\mu$m. The variation from a linear decrease in tension on the descending limb of the graph results from 1) the small number of contributing cross-bridges (~4 at full filament overlap: of 20 possible cross-bridges, this corresponds to 20% cross-bridge recruitment, a value consistent with that suggested by Howard (1997)), 2) changes in binding site registration, and 3) realignment of binding sites in response to cross-bridge forces, all of which depend on sarcomere length. Despite this variation from the monotonic decline observed in intact muscle preparations (Gordon et al., 1966), there is good agreement between the spatially explicit model and experimental data. Because mass action models do not account for filament geometry, these simulation results are unique to a spatially explicit model.

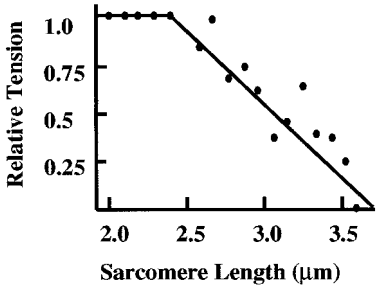


FIGURE 4 The predicted relative tension is plotted against sarcomere length for simulations that used the spring constants and geometric parameters shown in Fig. 3. The plateau of tension extends to ~2.3 $\mu$m. The tension declines to zero at a sarcomere length of 3.7 $\mu$m. Because of the misregistration of binding sites and myosin heads and because very few cross-bridges contribute to force production, there is some variation in the tension, and its decline is not cleanly linear.

## Force-velocity behavior

Simulations of force-velocity behavior show several intriguing results (Fig. 5). Our predictions exhibit a force-velocity behavior qualitatively similar to that shown experimentally: 1) we predict a maximum contraction velocity ($V_{max}$) of ~1.5 half-sarcomeres/s; 2) there is an inflection in the force-velocity curve at low shortening velocities, a prediction that is consistent with Edman's (1988) "double hyperbola" response for low shortening velocities; and 3) there is a marked increase in force, compared to the mass action prediction (*solid line* in Fig. 5), with active lengthening of fibers. Although predictions for $V_{max}$ can result from many traditional mass action kinetics models (e.g., Pate and Cooke, 1989; Piazzesi and Lombardi, 1995), the inflection of the force-velocity curve at low velocities and the increase in force during active lengthening have both been problematical (Harry et al., 1990). Thus the spatially explicit model is an improvement over mass action models in this regard.

As with our analyses of isometric tension above, binding site realignment plays a crucial role in our interpretation of the predicted force-velocity behaviors. The inflection of the force-velocity curve near low shortening velocities arises from the contribution of both motion-induced translocation of binding sites as well as a realignment of binding sites in response to cross-bridge forces. At these low shortening and lengthening velocities, the dynamics of force generation are dominated by this binding site rearrangement—forces are higher than predicted from our mass action model because

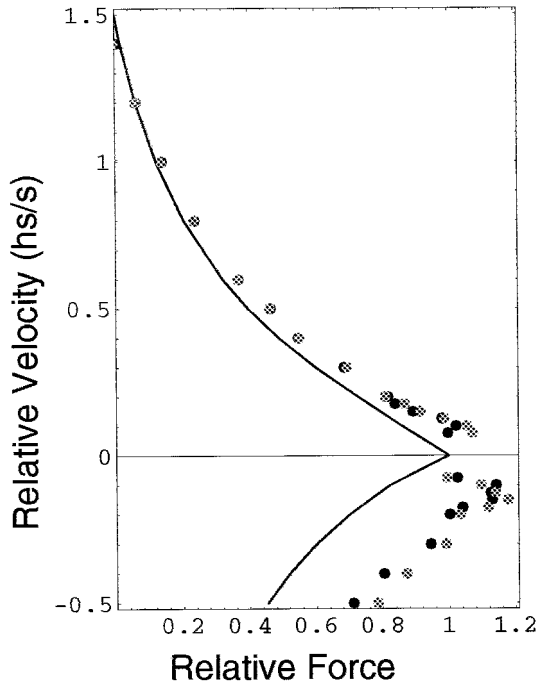


FIGURE 5 Model predictions for the force-velocity behavior are shown for three different simulations, all of which assume an initial sarcomere length of 2.5 $\mu$m: the curve corresponds to the force-velocity predictions of the mass action (partial differential equation) model, the black dots correspond to the Monte Carlo simulation with a thin filament spring constant of 1743 pN/nm, and the gray dots correspond to the Monte Carlo simulation with a thin filament compliance of 174.3 pN/nm. All of these simulations converge at large shortening velocities (low force), giving rise to a maximum shortening velocity of 1.5 half-sarcomere lengths/s. Significant deviation between the various models is seen at low shortening velocities (near isometric force). Filament compliance leads to greater force at low shortening velocities, with a change in the slope of the force velocity hyperbola that is consistent with Edman's (1988) observation. Furthermore, thin filament compliance leads to a significant increase in force for active lengthening. These increases in force are greater for the lower value of the thin filament spring constant (higher compliance).

there is an effective recruitment of binding sites to unbound cross-bridges. At high shortening velocities, the dynamics of strain-induced release of cross-bridges dominates observed dynamics. Here, predictions from the mass action and the spatially explicit models converge.

Compliance plays a crucial role here. Lower filament compliance leads to the mass action limit, with less increase in tension for active lengthening and a modest change in the inflection of the force-velocity behavior at low velocities. When compliance is increased to values that would mimic the 2-nm extension observed from x-ray data, the force-velocity behavior more closely approximates measured values.

### Tension transients in response to step changes in length

Rapid length transients applied to single muscle fibers have formed an experimental underpinning of our understanding of the cross-bridge cycle, giving rise to the classic T1 and T2 behaviors (Ford et al., 1977). These measures of mechanical responses are interpreted, respectively, as rapid redevelopment of tension by bound cross-bridges (on the order of milliseconds) followed by slower cycling of cross-bridges (Ford et al., 1977, 1981). Our simulations of rapid length perturbations also show behaviors qualitatively consistent with those reported experimentally (Fig. 6). Although the predictions for very large step changes in length deviate from observed behaviors, several crucial results arise from all of our analyses. In particular, tension recovery consists of two phases: an initial rapid increase in tension followed by a slower phase. In our results, the more rapid phase is associated with a 25% increase in the fraction of bound cross-bridges due to realignment of binding sites. In time, some of those that were bound before the length perturbation become negatively strained and, ultimately, release. This release of negatively strained cross-bridges is manifested as a rise in total tension. Thus, immediately after the length transient, the fraction bound initially rises and then declines.

## DISCUSSION

In this study we have examined the consequences of filament compliance with the dynamics of force generation by comparing two models: 1) a spatially explicit model of cross-bridge cycling in the context of local force balances within a compliant filament lattice, and 2) a simple mass action kinetics model that assumes zero compliance. A central issue here is that filament compliance leads to some level of dilation or compression of thin filament binding sites in response to cross-bridge forces. Therefore we asked whether, with observed estimates of filament and cross-bridge compliances, such redistribution of binding sites affects our interpretation of the force generation in muscle.

Our spatially explicit model successfully predicts a rather wide set of observed behaviors for contracting skeletal muscle that, in some instances, are beyond the predictive capacity of simple mass-action models. Filament strains, force-velocity behavior, and tension transients during step length changes all show predictions that encompass experimentally observed behaviors. In addition, two intriguing results emerge from the combined set of tests of the model. First, there is an important inhomogeneity in thin filament strain. Second, there is a realignment of binding sites in response to cross-bridge forces. Both of these issues can alter our present views of how cross-bridges generate force within the lattice of compliant filaments.

### Strain inhomogeneity

In isometric conditions, the strain inhomogeneity shown in Fig. 3 is present regardless of the amount of compliance within the filament. Its magnitude, however, is sensitive to the level of compliance, tending toward zero at zero fila-

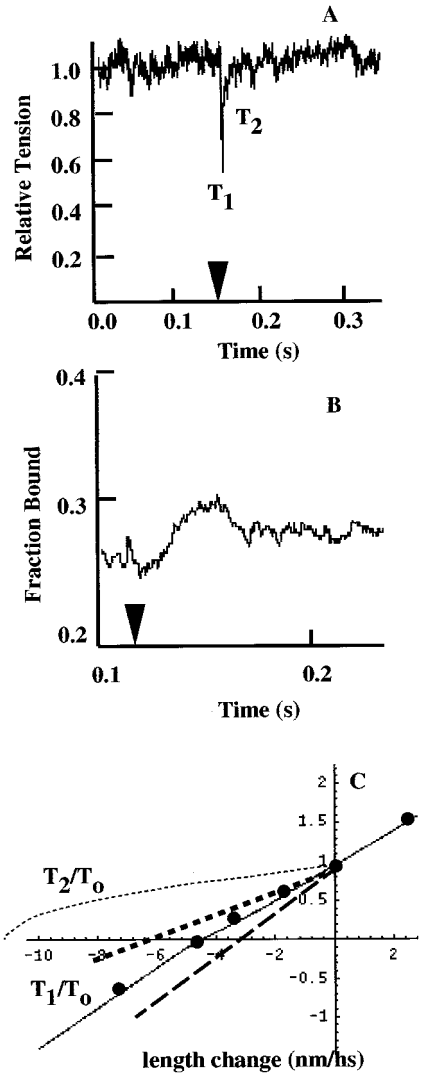


FIGURE 6 Predictions for rapid length transients derived from the average of 50 runs in which we used the geometric and mechanical properties summarized in Fig. 1. (*A*) The relative force for a step shortening of 2.5 nm per half-sarcomere plotted against time. These results show rapid tension recovery after T1 that precedes a slower recovery phase. (*B*) Plot of the instantaneous fraction of bound cross-bridges for an expanded time scale (0.1–0.2 s) to show an initial rise in cross-bridge binding followed by a decline. The slower decline in cross-bridge binding correlates with the slower rise in tension after T2. From these simulations of a variety of step changes in length, we computed the T1/To (*thin solid line*) and T2/To (*thin broken line*) behaviors (see Ford et al., 1981) and plotted them against the magnitude of the step length change (*C*). Also shown are the measured values (●) for T1/To from Ford et al. (1981). Our analysis captures much of the behavior shown by Ford et al. (1981), but T2/To is too high for large shortening steps. The T1/To behavior has an *x*-intercept that is consistent with experimentally observed values (Ford et al., 1981). Changes in thin filament compliance lead to changes in the T1/To behavior, with stiffer filaments having a steeper slope (10-fold stiffer; *thick long-dashed line*), and more compliant (10-fold less stiff) filaments having a shallower slope (*thick short-dashed line*).

ment compliance. For a compliance that would give rise to a 2-nm extension of the thin filament, as predicted by x-ray data (Huxley et al., 1994; Wakabayashi et al., 1994), we predict an inhomogeneous strain whose average is ~0.2% of the total sarcomere length. This inhomogeneity along the thin filament implies that cross-bridge forces are also nonuniform along each of the filaments. Large spatial changes in strain correspond to large forces. Thus the dynamics of cross-bridge cycling, as mediated by binding availability, must also vary along the thin filament. Indeed, it is possible to have higher cross-bridge cycling near the free end of the filament, where forces are lower and binding site movements are larger. Thus the assumption implicit in mass action models that cycling does not vary along any one filament is contradicted by this observation.

Although strain inhomogeneities are clearly important, their magnitude is sensitive to the values for filament spring constants and those for the cross-bridges. Unfortunately, there appears to be some uncertainty about these: direct force measurements of thin filaments can vary by a factor of 3 (Kojima et al., 1994; Isambert et al., 1995). These, along with uncertainty in cross-bridge spring constants, confound a clear prediction of the actual level of strain with the filament. We have also argued that accounting for the geometry of the filament lattice is crucial in understanding how x-ray data for thin filament distortion can be explained in the context of direct measurement of thin filament mechanical properties. However, in the current form of our model—a highly reduced geometry of just two interacting filaments—we can only indicate a critical role for compliance in determining force generation. A fuller, three-dimensional model would be required for a more complete understanding of the spatial distribution of forces within the filament lattice. Nevertheless, even with our simple filament geometry, we are able to show that the strain inhomogeneity resulting from filament compliance introduces a functionally important mechanical coupling between cross-bridge cycling and the spatial distribution binding sites.

## Compliant realignment of binding sites

A fundamental phenomenon underlying all of the simulations, regardless of our uncertainty with spring constants, is that binding sites rearrange in response to cross-bridge forces. The consequences of this compliant realignment of binding sites (CRB) follows from the unequal spacing of cross-bridges and binding sites (unstrained, ~43 nm in the thick filament and ~37 nm in the thin filament; Gordon, 1989). Without force generation, only a small fraction of the cross-bridges are actually within 2 nm of a binding site and thus have binding probabilities that exceed 0.1. Thus, for a rigid filament model considered here, only a small fraction of cross-bridges can be bound at any time. Whereas Mijailovich et al. (1996) predict rather high binding probabilities (reaching 1.0), our results suggest otherwise. However, when one cross-bridge binds, CRB makes available binding sites that were previously inaccessible to other unbound cross-bridges. Similarly, CRB will alter the kinetics of

cycling between the bound states and the kinetics of detachment, because these transitions depend upon the local strain of any one cross-bridge. That CRB strongly determines the mechanical events underlying muscle contraction raises concerns about how we interpret mechanical transients in light of cross-bridge theories.

CRB modulates the dynamics of the force-velocity behavior and rapid length transients. In the former case, CRB gives rise to an inflection in the slope of the force-velocity curve at low velocities (Fig. 5). This inflection arises from the realignment of binding sites, bringing into view those that were previously inaccessible to otherwise unbound cross-bridges. Similarly, this realignment helps explain tension transients that follow from rapid length changes (Fig. 6). Here, too, binding site motions modulate cross-bridge cycling. In this latter case, a rapid increase in tension follows from CRB, again with previously inaccessible binding sites becoming available to otherwise unbound cross-bridges. As noted above, the slower rise in tension follows from the release of bound cross-bridges that became negatively strained after the rapid recruitment of new cross-bridges to the population. These model predictions are generally consistent with experimental studies suggesting that the detachment dynamics of cross-bridges are important components of tension redevelopment after rapid length changes (Piazzesi et al., 1997; Seow et al., 1997).

If CRB is generally important to muscle function, then filaments may be either too compliant or too stiff for effective force generation. We addressed this issue by simulating the maximum isometric tension generation as a function of both thin filament and cross-bridge spring constants (Fig. 7). Our results show mechanical tuning with an ensemble of motor molecules coupled in a lattice of compliant filaments. Such tuning follows from two key issues. First, filaments with low compliance do not permit appreciable CRB and, as such, lead to generally lower binding and force production. However, if filament compliance is too great, extensive CRB leads to situations in which cross-bridges do work upon each other, reducing the total force. Similarly, cross-bridges that are too stiff may not have sufficient mobility to find binding sites with a reasonable probability (see Eq. 6a); those that are too compliant may bind with high probability, but do so with little force production.

The peak value of tension (Fig. 7) occurs when the local spring constant of the thin filament is ~250 pN/nm. This value is lower than our estimate of 1743 pN/nm (for a 37.3-nm-long piece of thin filament) on the basis of the data from Kojima et al. (1994). But, as we noted earlier, there are cross-bridges from three thick filaments acting on each thin filament. Furthermore, the data from Isambert et al. (1995) indicate another factor of 2 or 3 in decreasing thin filament stiffness due to calcium activation. Thus the tuning peak occurs where the thin filament compliance would be high enough to capture the thin filament deformations measured by Huxley et al. (1994) and Wakabayashi et al. (1994).

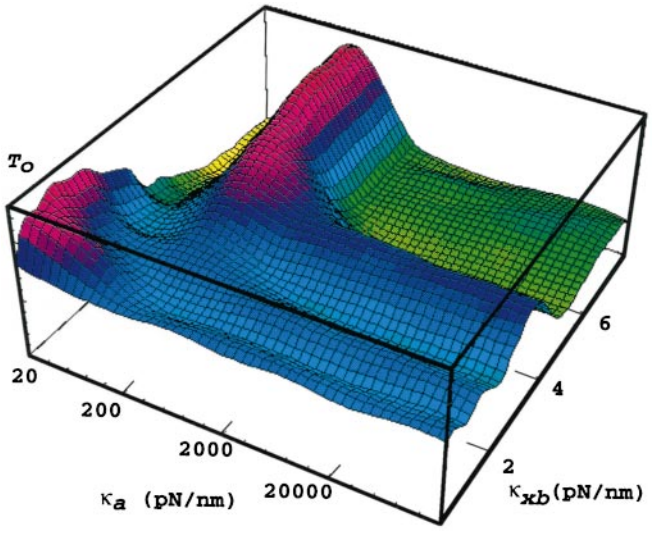


FIGURE 7 Mechanical tuning of a sarcomere with compliant filaments. Tension is plotted against the thin filament spring constant ($\kappa_a$) and the cross-bridge spring constant ($\kappa_{xb}$). There is a sharp peak in tension generation that follows from compliant realignment of binding sites: thin filaments with high $\kappa_a$ do not permit additional recruitment of cross-bridges, whereas those with low $\kappa_a$ deform to an extent that releases the strain in cross-bridges. The tuning peak corresponds to a thin filament spring constant of ~250 pN/nm, a value 10 times lower than that reported by Kojima et al. (1994), but one that gives strain predictions consistent with those estimated by Huxley et al. (1994) and Wakabayashi et al. (1994) (see Fig. 3).

Our results suggest that mechanical tuning emerges from the ensemble of kinetic and mechanical events within the lattice of muscle proteins. Significant deviations from the range of observed mechanical properties may have profound consequences for the performance of contractile systems. Although the compliances of thin filaments, thick filaments, and cross-bridges may be rather conservative, the linear arrangement of these elastic springs suggests an intriguing mechanism by which natural variation in the geometry of the sarcomere may strongly influence both the tuning and dynamics of force generation. For example, a series of thin filament springs ($k_a$ = 1743 pN/nm), each 37 nm long, yields a total spring constant of ~65 pN/nm for a thin filament 1 $\mu$m long (see above). This total spring constant decreases linearly with increasing filament length (= $k_a/M$). Therefore, the total distortion induced by cross-bridge forces will depend upon thin filament length, and accordingly, the shape of the tuning curve and the dynamics of cycling will depend upon a parameter that varies significantly across species and muscle types (thin filament lengths vary from 0.3 to 6 $\mu$m; Hoyle, 1983).

The authors gratefully acknowledge Drs. A. M. Gordon, M. Kushmerick, M. Regnier, and D. Martyn. Assistance from J. Sherman, E. Stockwell, M. Frye, and M. Tu is greatly appreciated.

This work was supported by grants from the National Science Foundation (IBN 9511681) and the National Institutes of Health (HL 52558).

## REFERENCES


Bagni, M. A., G. Cecchi, F. Colomo, and C. Peggesi. 1990. Tension and stiffness of frog muscle fibres at full filament overlap. *J. Mus. Res. Cell Motil*. 11:371–377.

Bird, R. B., W. E. Stewart, and E. N. Lightfoot. 1960. Transport Phenomena. John Wiley and Sons. New York.

Chase, P. B., and M. J. Kushmerick. 1995. Effect of physiological ADP levels on contraction of single skinned fibers from rabbit fast and slow muscles. *Am. J. Physiol.* 268:C480–C489.

Córdova, N. J., B. Ermentrout, and G. Oster. 1992. Dynamics of single-motor molecules: the thermal ratchet model. *Proc. Natl. Acad. Sci. USA*. 89:339–343.

Crow, M. T., and M. J. Kushmerick. 1982. Chemical energetics of slow- and fast-twitch muscle of the mouse. *J. Gen. Physiol.* 79:147–166.

Dantzig, J., Y. E. Goldman, N. Lacktis, and E. Homsher. 1992. Reversal of the cross-bridge force-generating transition by photogeneration of phosphate in rabbit psoas muscle fibers. *J. Physiol. (Lond.)*. 451:247–278.

Edman, K. A. P. 1988. Double-hyperbolic force-velocity relation in frog muscle fibres. *J. Physiol. (Lond.)*. 404:301–321.

Fichthorn, K. A., and W. H. Weinberg. 1991. Theoretical foundations of Monte Carlo simulations. *J. Chem. Phys*. 95:1090–1096.

Finer, J. T., R. M. Simmons, and J. A. Spudich. 1994. Single myosin molecule mechanics: piconewton forces and nanometre steps. *Nature*. 368:113–119.

Ford, L. E., A. F. Huxley, and R. M. Simmons. 1977. Tension responses to sudden length changes in stimulated frog muscle fibres near slack length. *J. Physiol. (Lond.)*. 269:441–515.

Ford, L. E., A. F. Huxley, and R. M. Simmons. 1981. The relationship between stiffness and filament overlap in stimulated frog muscle fibres. *J. Physiol. (Lond.)*. 311:219–249.

Glynn, H., and J. Sleep. 1985. Dependence of adenosine triphosphate activity of rabbit psoas muscle fibres and myofibrils on substrate concentration. *J. Physiol. (Lond.)*. 365:259–276.

Goldman, Y. E., and A. F. Huxley. 1994. Actin compliance: are you pulling my chain? *Biophys. J.* 67:2131–2133.

Gordon, A. M., A. F. Huxley, and F. J. Julian. 1966. The variation in isometric tension with sarcomere length in vertebrate muscle fibres. *J. Physiol*. 184:170–192.

Harry, J. D., A. W. Ward, N. C. Heglund, D. L. Morgan, and T. A. McMahon. 1990. Cross-bridge cycling theories cannot explain high-speed lengthening behavior in frog muscle. *Biophys. J.* 57:201–208.

Higuchi, H., T. Yanagida, and Y. E. Goldman. 1995. Compliance of thin filaments in skinned fibers of rabbit skeletal muscle. *Biophys. J.* 69: 1000–1010.

Homsher, E., and J. Lacktis. 1988. The effects of shortening on the phosphate release step of the actomyosin ATPase mechanism. *Biophys. J.* 53:564a.

Howard, J. 1997. Molecular motors: structural adaptations to cellular functions. *Nature.* 389:561–567.

Hoyle, G. 1983. Muscles and Their Neural Control. Wiley, New York.

Hunt, A. J., F. Gittes, and J. Howard. 1994. The force exerted by a single kinesin molecule against a viscous load. *Biophys. J.* 67:766–781.

Huxley, A. F., and R. M. Simmons. 1971. Proposed mechanism of force generation in striated muscle. *Nature*. 233:533–538.

Huxley, H. E., A. Stewart, H. Sosa, and T. Irving. 1994. X-ray diffraction measurements of the extensibility of actin and myosin filaments in contracting muscle. *Biophys. J.* 67:2411–2421.

Isambert, H. P., A. C. Venier, A. Maggs, A. Fattoum, R. Kassab, D. Pantaloni, and M. R. Carlier. 1995. Flexibility of actin filaments derived from thermal fluctuations: effect of bound nucleotide, phalloidin, and muscle regulatory proteins. *J. Biol. Chem.* 270:11437–11444.

Kojima, H., A. Ishijima, and T. Yanagida. 1994. Direct measurement of stiffness of single actin filaments with and without tropomyosin by in vitro nanomanipulation. *Proc. Natl. Acad. Sci. USA.* 91:12962–12966.

Kramers, H. A. 1940. Brownian motion in a field of force and the diffusion model of chemical reactions. *Physica*. 7:284–304.

Kushmerick, M. J., T. S. Moerland, and R. W. Wiseman. 1992. Mammalian skeletal muscle fibers distinguished by contents of phosphocreatine, ATP, and Pi. *Proc. Natl. Acad Sci. USA*. 89:7521–7525.

Mijailovich, S. M., J. J. Fredberg, and J. P. Butler. 1996. On the theory of muscle contraction: filament extensibility and the development of isometric force and stiffness. *Biophys. J.* 71:1475–1484.

Molloy, J. E., J. E. Burns, J. Kendrick-Jones, R. T. Tregear, and D. C. S. White. 1995a. Movement and force produced by a single myosin head. *Nature*. 378:209–212.

Molloy, J. E., J. E. Burns, J. C. Sparrow, R. T. Tregear, J. Kendrick-Jones, and D. C. S. White. 1995b. Single-molecule mechanics of heavy meromyosin and S1 interacting with rabbit or *Drosophila* actins using optical tweezers. *Biophys. J.* 68:298–305.

Papoulis, A. 1991. Probability, Random Variables, and Stochastic Processes. McGraw-Hill, New York. 348–351.

Pate, E., and R. Cooke. 1989. A model of cross-bridge actions: the effects of ATP, ADP, and $P_i$. *J. Muscle Res. Cell Motil.* 10:181–196.

Piazzesi, G., M. Linari, M. Reconditi, F. Vanzi, and V. Lombardi. 1997. Cross-bridge detachment and attachment following a step stretch imposed on active single frog muscle fibers. *J. Physiol. (Lond.)*. 498:3–15.

Piazzesi, G., and V. Lombardi. 1995. A cross-bridge model that is able to explain mechanical and energetic properties of shortening muscle. *Biophys. J.* 68:1966–1979.

Press, W. H., S. A. Teukolsky, W. T. Vetterling, and B. P. Flannery. 1992. Numerical Recipes in C: The Art of Scientific Computing. Cambridge University Press, Cambridge.

Seow, C. Y., S. G. Shroff, and L. E. Ford. 1997. Detachment of low-force bridges contributes to the rapid tension transients of skinned rabbit skeletal muscle fibres. *J. Physiol. (Lond.)*. 501:149–164.

Wakabayashi, K., Y. Sugimoto, H. Tanaka, Y. Ueno, Y. Takezawa, and Y. Amemiya. 1994. X-ray diffraction evidence for the extensibility of actin an myosin filaments during muscle contraction. *Biophys. J.* 67: 2422–2435.